ELSEVIER

Lock-In Behavior in Simulated Vortex-Induced Vibration

Hugh Blackburn
CSIRO Division of Building, Construction and Engineering, Highett, Australia

Ron Henderson
Graduate Aeronautical Laboratories, California Institute of Technology, Pasadena, California

■ Results are presented for a two-dimensional numerical simulation of vortex-induced vibration of a circular cylinder at a Reynolds number of 250. A spectral element spatial discretization and a stiffly stable time integration scheme were employed to solve the Navier–Stokes equations in an accelerating frame of reference attached to the cylinder. The response envelope of the vibrating cylinder was similar to those previously obtained in experiments, and lock-in (coalescence of cross-flow oscillation and vortex-shedding frequencies at a frequency close to the cylinder natural frequency) was observed. Chaotic cylinder responses were observed over a range of cylinder natural frequencies. Simulations of flows past a cylinder in forced cross-flow oscillation are also discussed, and a result showing an asymmetric $P + S$ vortex shedding mode is presented.

Keywords: *cylinder, vortex, vibration, lock-in, wake, chaos*

INTRODUCTION

The problem of vortex-induced vibration of slender flexible structures in cross flow holds considerable theoretical and practical interest. Partly as a response to the difficulties of setting up and obtaining useful measurements from an experimental investigation into the problem, we have taken a computationally based approach. Although at present the range of Reynolds numbers for direct numerical simulation is comparatively limited, especially for three-dimensional computations, much useful information concerning the physics of the body–wake interaction may be obtained. The restriction may not be too important, since, as has been noted many times, the physics of vortex shedding and fluid–structure interaction seem to be broadly similar over the observed range of Reynolds numbers above 100 despite the many Reynolds transitions that may affect the details of the flow. It is also generally accepted that near-wake flow structures become increasingly two-dimensional as body vibration amplitudes increase.

In a previous study [1], results were presented for forced and free cylinder oscillation at Re = 200 and convergence studies were discussed. The lock-in phenomenon and the rapid change of phase of vortex shedding with change in cylinder oscillation frequency [2] were both observed for forced cross-flow oscillations. In addition, the approach to a limiting maximum amplitude of oscillation in free vibration as Scruton's mass-damping parameter $4\pi\zeta m/\rho D^2 \rightarrow 0$ was observed for the single value of cylinder natural frequency investigated there, mimicking experimental behavior (e.g., Griffin [3]).

In the first part of this paper we concentrate on free vibration behavior. The mean flow speed (i.e., Reynolds number) was held constant, and the natural frequency of the cylinder was varied between runs; each run was restarted using cylinder state parameters and flow field obtained at the end of the previous run. In most cases, simulations were run for a dimensionless time $tU/D = 300$ or approximately 60 periods of vortex shedding for the fixed cylinder (Strouhal number St = 0.2077). This was usually sufficient to obtain a steady-state oscillation. The cylinder damping ratio was held constant at $\zeta = 0.01$, while the cylinder mass per unit length was also held constant with $m/\rho D^2 = 10$, to give $4\pi\zeta m/\rho D^2 = 1.2566$. For results presented here, cylinder natural frequency was increased in small steps between successive runs.

In the latter part of the paper, attention is turned to examination of wake modes in vortex-induced and forced oscillation, since symmetrical and asymmetrical vortex interaction in the near wake is an important feature of cylinder–wake coupling [6, 7].

PROBLEM FORMULATION

The computational domain Ω employed for the two-dimensional simulations is shown in Fig. 1; the domain extended a distance of $12.5D$ upstream and cross-flow from the cylinder centerline, and a distance of $25D$ downstream. A large cross-flow mesh dimension was employed to minimize blockage effects. Prescribed-velocity boundary conditions were used on the inflow, upper and lower boundaries, while at the downstream end of the domain,

Address correspondence to Hugh Blackburn, CSIRO Division of Building, Construction and Engineering, P.O. Box 56, Highett, Vic 3190, Australia.

Experimental Thermal and Fluid Science 1996; 12:184–189

655 Avenue of the Americas, New York, NY 10010

0894-1777/96/$15.00
SSDI 0894-1777(95)00093-3

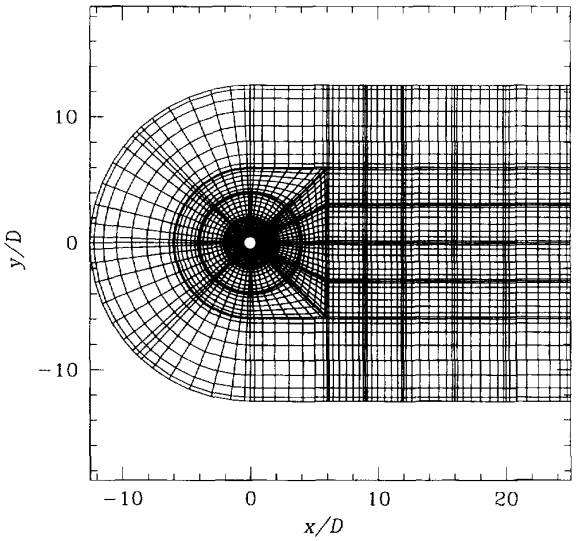

Figure 1. Gauss–Legendre–Lobatto spectral element mesh for domain Ω employed in the free vibration calculations. Each of the elements closest to the cylinder has thickness $0.1D$.

outflow velocity and pressure boundary conditions were used.

The numerical and physical treatment of the problem in two and three dimensions has been previously described by Blackburn and Karniadakis [1] and references therein. The physical formulation is briefly re-presented below for completeness.

Rather than arrange a method in which the computational grid deformed to allow cylinder motion, we have used a fixed-configuration grid attached to the cylinder. By applying appropriate boundary conditions and adding a fictitious forcing term to the Navier–Stokes equations, the flow simulation may be carried out in this accelerating reference frame. The incompressible Navier–Stokes equations, written in rotational form for an inertial reference frame, are

$$\frac{\partial \mathbf{u}}{\partial t} = -\nabla \Pi + \mathbf{u} \times \boldsymbol{\omega} + \nu \nabla^2 \mathbf{u}, \tag{1}$$

where $\Pi = p/\rho + \mathbf{u} \cdot \mathbf{u}/2$ and $\boldsymbol{\omega} = \nabla \times \mathbf{u}$. If the reference frame in which the Navier–Stokes equations are solved has a rectilinear acceleration $\mathbf{a}$, then the equations become

$$\frac{\partial \mathbf{u}}{\partial t} = -\nabla \Pi + \mathbf{u} \times \boldsymbol{\omega} + \nu \nabla^2 \mathbf{u} - \mathbf{a}. \tag{2}$$

The appropriate velocity boundary conditions at prescribed-velocity boundaries are

$$\mathbf{u} = -\mathbf{v}, \tag{3}$$

where $\mathbf{v}$ is the velocity of the reference frame. The corresponding pressure boundary condition is obtained by taking the normal component of (2), generated by dotting the unit normal boundary vector $\mathbf{n}$ into (2) to make

$$\frac{\partial \Pi}{\partial n} = \mathbf{n} \cdot [\mathbf{u} \times \boldsymbol{\omega} - \nu \nabla \times \boldsymbol{\omega}], \tag{4}$$

where the form of the viscous term follows the suggestion of Orszag et al. [4]. On the body boundary,

$$\frac{\partial \Pi}{\partial n} = \mathbf{n} \cdot [\mathbf{u} \times \boldsymbol{\omega} - \nu \nabla \times \boldsymbol{\omega} - \mathbf{a}]. \tag{5}$$

The force per unit length exerted by the pressure field on the cylinder is given by

$$\mathbf{f}_p = \oint p\mathbf{n}\, ds = \oint \rho \Pi \mathbf{n}\, ds, \tag{6}$$

where $\mathbf{n}$ is again the unit outward normal of the fluid domain and the integration is performed around the circumference of the cylinder, while the viscous force per unit length is

$$\mathbf{f}_v = -\oint \mu \mathbf{n} \cdot [\nabla \mathbf{u} + (\nabla \mathbf{u})^T]\, ds. \tag{7}$$

If the cylinder undergoes forced oscillation, the velocity and acceleration of the reference frame are given. However, in the case of free vibration the mass, stiffness, and damping of the cylinder must be considered, and second-order ODEs of the form

$$\ddot{\mathbf{x}} + 2\zeta \omega_n \dot{\mathbf{x}} + \omega_n^2 \mathbf{x} = \mathbf{f}/m \tag{8}$$

must be solved for each axis of motion, where for two-dimensional calculations m is the cylinder mass per unit length and $\mathbf{f} = \mathbf{f}_p + \mathbf{f}_v$ is the total force per unit length exerted by the fluid. Following normal practice, these are decomposed into a set of first-order ODEs with $\mathbf{v} = \dot{\mathbf{x}}$, giving

$$\begin{aligned} \dot{\mathbf{v}} &= \mathbf{f}/m - 2\zeta \omega_n \mathbf{v} - \omega_n^2 \mathbf{x}, \\ \dot{\mathbf{x}} &= \mathbf{v}. \end{aligned} \tag{9}$$

Here $\mathbf{v}$ is identical with the reference frame velocity, as it is fixed to the cylinder.

Equations (2) are solved together with the incompressibility constraint

$$\nabla \cdot \mathbf{u} = 0 \qquad \text{in } \Omega. \tag{10}$$

As discussed in Blackburn and Karniadakis [1], a spectral element spatial discretization with a conforming Gauss–Legendre–Lobatto mesh was combined with a stiffly stable time integration scheme based on backward differencing to solve (2) and (10) using primitive variables. The same stiffly stable scheme was used to integrate (9) to obtain the motion of the cylinder. The domain was modeled using 86 macroelements, each with eighth-order tensor product Gauss–Legendre–Lobatto interpolants for the velocity and pressure fields.

RESULTS: VORTEX-INDUCED VIBRATION RESPONSE

A diagram showing the cylinder response amplitudes and frequencies together with mean drag and fluctuating lift forces is presented in Fig. 2, where the changes of cylinder natural frequency in vacuo (f_n) are characterized by the ratio f_n/f_v, where f_v is the vortex-shedding frequency for the fixed cylinder.

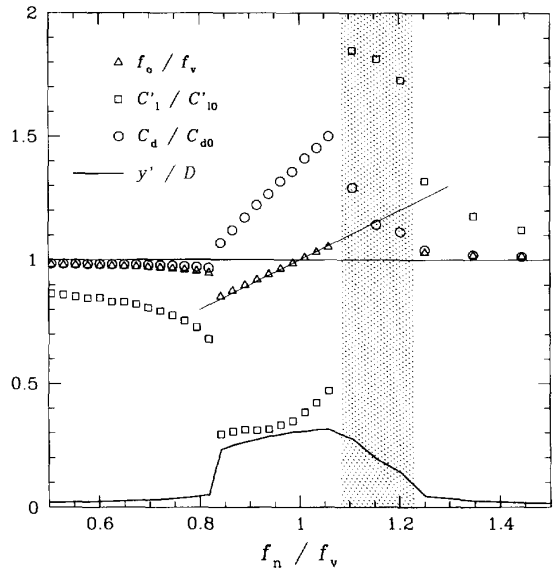

Figure 2. Cylinder response diagram. Values along the abscissa represent the ratio of cylinder in vacuo natural frequency f_n to Strouhal frequency for the fixed cylinder f_v. (□) Ratio of fluctuating lift coefficients C'_l/C'_{l_0}; (○) ratio of mean drag coefficients C_d/C_{d_0}; (△) ratio of oscillation frequency to fixed-cylinder Strouhal frequency f_o/f_v; (—) standard deviation of cylinder cross-flow response amplitude y'/D. Shaded region indicates chaotic regime.

An example showing transient cylinder response at the onset of lock-in ($f_n/f_v = 0.843$) is shown in Fig. 3. Note that the scale of along-flow response (x/D) is greatly exaggerated compared to the cross-flow response.

Cylinder Oscillation Frequency and Amplitude

For all the simulations, cylinder cross-flow oscillation and lift frequencies were found to coincide at steady state. However, the lift/oscillation frequency f_o was nearly the same as f_v away from $f_n/f_v = 1$. Near $f_n/f_v = 1$ both frequencies changed together to fall near (but not exactly on) f_n; exact coincidence with f_n is indicated by the slanted thin line near the center of Fig. 2. This change in vortex-shedding frequency to nearly match the cylinder natural frequency is the lock-in phenomenon. During lock-in, amplitudes of cross-flow oscillation increased markedly: the largest steady-state values correspond to peak-to-peak oscillation amplitudes of approximately $0.9D$ (standard deviation values of y/D are presented in Fig. 2). Note that while the cylinder was free to oscillate in the along-flow direction, only cross-flow amplitudes are reported here; typically the fluctuating along-flow response was an order of magnitude smaller than for cross flow. The lack of exact coincidence of f_o with f_n during lock-in can be accounted for by a phase difference between cylinder motion and lift forces, which is known to be a function of f_n/f_v.

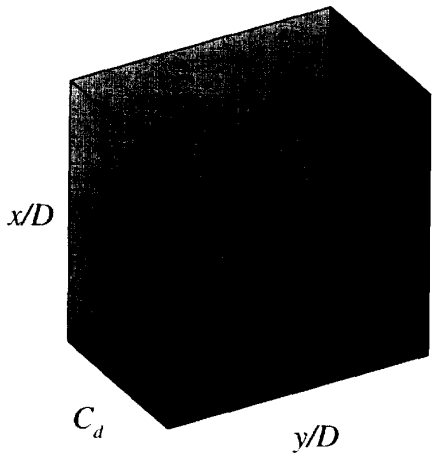

Figure 3. Transient cylinder response at the onset of lock-in, $f_n/f_v = 0.843$. C_d increases into the page; x/D increases down the page. The progression to large-amplitude lock-in oscillations was accompanied by a decrease in the mean value of x/D, corresponding to an increase in f_n (increasing stiffness).

Lift and Drag

For the fixed cylinder, $C_{d_0} = 1.446$, $C'_{d_0} = 0.0452$, and $C'_{l_0} = 0.581$. Values for the oscillating cylinder are presented in Fig. 2 as ratios of the values for the fixed cylinder. Coinciding with the onset of lock-in at $f_n/f_v \simeq 0.825$, mean drag coefficients began to rise above values for the stationary cylinder. More notable were the large drop in fluctuating lift coefficients and the steady drop at frequencies below lock-in, emphasizing that even small amplitudes of response can substantially affect the vortex-shedding process. The behavior of lift and drag coefficients during lock-in was similar to that observed in the forced-vibration results presented in Fig. 3 of Blackburn and Karniadakis [1].

Chaotic Response Regime

At frequency ratios of 1.11–1.20, above lock-in, chaotic cylinder responses were observed, as shown, for example, in Fig. 4 for frequency ratio $f_n/f_v = 1.11$; the autospectrum of the time series is presented in Fig. 5. The responses are described as chaotic because they are aperiodic (Fig. 4) and display noisy spectra (Fig. 5) with two peaks that are not related in any simple way to the sum and difference frequencies of the fixed-cylinder vortex shedding frequency and the cylinder natural frequency.

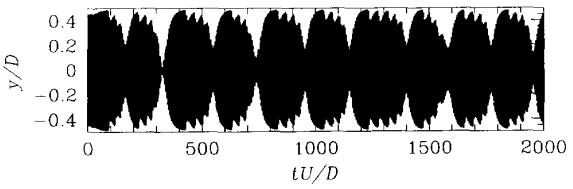

Figure 4. Chaotic cross-flow response for $f_n/f_v = 1.11$.

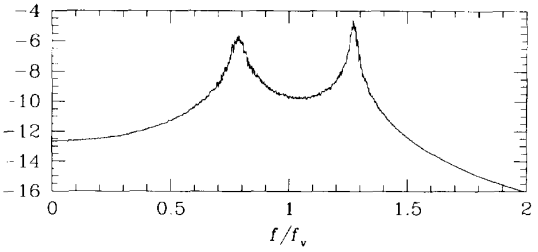

Figure 5. Autospectrum of cross-flow response for $f_n/f_v = 1.11$. Spectral peaks are incommensurate with the cylinder natural frequency and the fixed-cylinder Strouhal frequency.

Both the cylinder response and the motion of the wake are chaotic.

To ensure that these observations were not due to transient effects, the simulation times were extended to 700 and then 2000 (400 vortex shedding cycles). The chaotic responses were due to an intermittent lock-in effect. Phase-space visualization of cylinder state variables (as in Fig. 3) showed that during times when the cylinder amplitudes were large, responses approached the typical limit cycle for the lock-in regime (similar to a Lissajous figure). Entry to the chaotic state also produced a substantial increase in standard deviation lift coefficients to almost double the values for the fixed cylinder. We intend to make a more detailed study of this regime, following the suggestion of Van Atta and Gharib [5].

RESULTS: FLOW VISUALIZATION AND WAKE MODES

It was of interest in the present simulations to examine wake flow structures, particularly as they may affect the lock-in process. The work of Brika and Laneville [6] suggests that the lock-in regime might be associated with a change in vortex shedding modes, for example from the normal shedding of a single pair of vortices for each cycle of cylinder motion away from lock-in to the shedding of two pairs of vortices per cycle. This effect was first noted in the forced-oscillation experiments of Williamson and Roshko [7], where these two modes were called 2S and 2P, respectively. Williamson and Roshko also noted asymmetric wake modes, with paired vortices on one side of the wake and single-signed vortices on the other; these were called P + S modes. In the free-vibration experiments of Brika and Laneville, the 2P mode was found to be associated with large-amplitude responses in the lock-in regime. [Note the similarity between the response envelope for y'/D in Fig. 2 here and the lower plateau in Fig. 19 of Brika and Laneville (after accounting for the fact that the senses of the abscissas are reversed).]

Since the presence of wake vortices should be indicated in the solution vorticity field, we produced animations of ω contours derived from the simulation results for a cycle of oscillation in the lock-in regime for different values of the ratio f_n/f_v. In all the vortex-induced vibration results we obtained at Re = 250, only the regular 2S mode was observed. While there is some difficulty in directly comparing flow structures obtained by visualization using instantaneous streaklines (short time exposures of particle paths; Williamson and Roshko), streaklines (smoke particles released from cylinder surface; Brika and Laneville), and vorticity field/instantaneous streamlines, the present results for the vorticity field should be able to differentiate between the 2S and 2P modes. The implication is that the 2P mode is not necessarily associated with the large-amplitude response plateau in the lock-in regime.

Williamson and Roshko's published results [7] were obtained at Reynolds numbers generally in the range 500–1000, whereas the present set of results in vortex-induced vibration were obtained at Re = 250. Hence it was initially conjectured that the lack of 2P or P + S modes in the simulation results might be attributed to greater diffusivity of vorticity at the lower Reynolds numbers, and simulations are presently under way at Re = 500. Subsequently, Williamson (1994, private communication) provided a streakline photograph of the P + S mode in forced cross-flow oscillations at Re = 140, with cross-flow peak amplitude of $\pm 0.6D$ ($y'/D = 0.42$) and $f_o/f_v = 0.152$. This result is shown here as Fig. 6. The flow is assumed to be nearly two-dimensional, as it is for a fixed cylinder at these Reynolds numbers, although the photograph does provide some indication of three-dimensional flow.

We were initially unable to obtain a P + S mode for forced cross-flow oscillation at Re = 140, starting the oscillation at an amplitude of $\pm 0.6D$ in a flow field established with a fixed cylinder. However, we found that at higher amplitudes of oscillation the P + S mode appeared, and we were able to maintain it at lower amplitudes (thus far, down to $\pm 0.75D$ or $y'/D = 0.53$). A plot of vorticity field contours resulting from the simulation is shown in Fig. 7; the similarity to the flow visualization of Fig. 6 is striking. By changing initial conditions, it may be possible to hold the P + S mode down to lower amplitudes, matching those of Williamson. The presence of wake modes other than the conventional 2S mode in vortex-induced vibration (as opposed to forced oscillation) at low Reynolds numbers is still an open question.

PRACTICAL SIGNIFICANCE

Vortex-induced vibration of slender circular-cylindrical structural elements is an important consideration for the fabrication, transport, and operational design phases of many offshore structures. Despite the relatively fundamental nature of the problem, a comparatively small amount is known about the nature of the fluid–structure interaction, and the design rules that exist (e.g., CIRIA [8]) are based on a limited set of experimental results, such as those reviewed by King [9]. Partly as a result of the lack of understanding of the phenomenon, apparently unrelated sets of design procedures are available for structures immersed in flows of water (e.g., CIRIA) and air (e.g., ESDU [10]). The present computational approach to investigation of this fluid–structure interaction problem should enhance understanding of the phenomenon, leading to more rational design rules and suggesting new approaches to its control.

Figure 6. Dye-marked streaklines in forced cross-flow oscillation at Re = 140, $y'/D = 0.42$, $f_o/f_v = 0.152$, demonstrating the P + S wake mode. (Photograph courtesy of C. H. K. Williamson, Cornell University.)

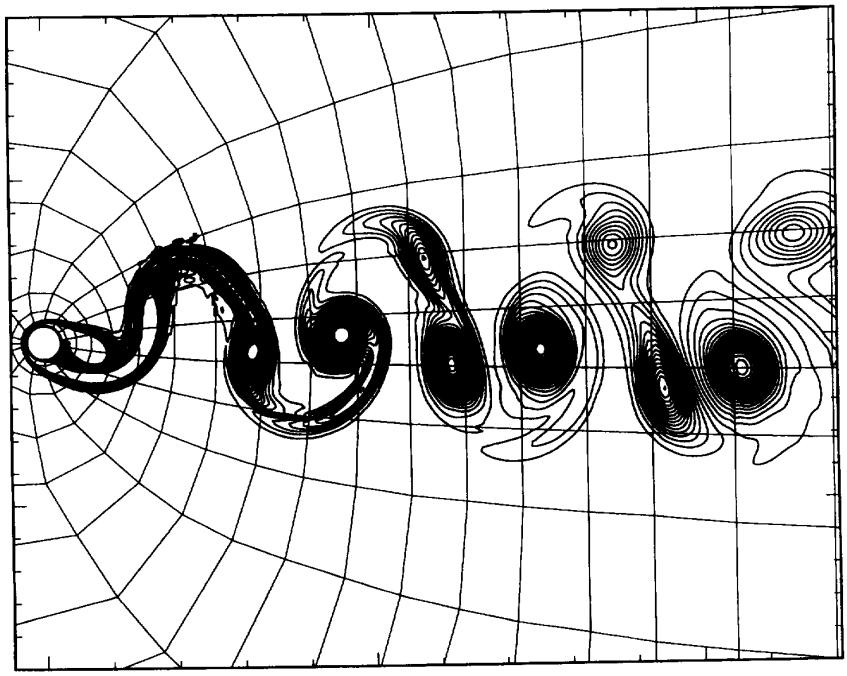

Figure 7. Vorticity contours in simulation of forced cross-flow oscillation at Re = 140, $y'/D = 0.53$, $f_o/f_v = 0.152$. Compare with experimental flow visualization of Fig. 6.

CONCLUSIONS

The simulation results show that the numerical method is able to reproduce many of the vortex-induced vibration phenomena obtained in experiments. The ready availability of detailed results such as lift and drag coefficients, flow field, and body state variables, emphasizes the power and utility of the computational approach to the problem of vortex-induced vibration. We intend to pursue the issues of low-dimensional modeling of the cylinder–wake system and near-wake transport properties (as discussed by Shariff et al. [11]), but a more pressing need is to understand the physics that underlies lock-in behavior.

An important extension of the present simulation technique is to three-dimensional flows. Use of Fourier transform techniques in the homogeneous (spanwise) direction facilitates parallel computations, as outlined in [1]. We have carried out a set of example three-dimensional calculations for a freely vibrating cylinder at Re = 250, and the use of unstructured spectral element methods [12] should enable us to expand the Reynolds number envelope of direct numerical simulations to Re $\simeq$ 1000 with present computational resources.

Part of this work was performed while H.B. was employed by Monash University and on secondment to Princeton University. Additional support was provided by the Australian Research Council and the Office of Naval Research. We thank Professor George Karniadakis for his continued interest and support.

NOMENCLATURE

- $\mathbf{a}$ reference frame acceleration vector, m/s^2
- C_d drag coefficient ($= F_d/0.5\rho U^2 D$), dimensionless
- C_l lift coefficient ($= F_l/0.5\rho U^2 D$), dimensionless
- D cylinder diameter, m
- F_d drag force per unit length, kg/s^2
- F_l lift force per unit length, kg/s^2
- f_n cylinder in vacuo natural frequency, Hz
- f_o cylinder oscillation frequency, Hz
- f_v vortex shedding frequency for fixed cylinder, Hz
- $\mathbf{f}$ force per unit length exerted on cylinder by fluid, kg/s^2
- $\mathbf{f}_p$ pressure force per unit length exerted on cylinder by fluid, kg/s^2
- $\mathbf{f}_v$ viscous force per unit length exerted on cylinder by fluid, kg/s^2
- m cylinder mass per unit length, kg/m
- $\mathbf{n}$ unit outward normal vector, m
- p pressure, kg/m s^2
- Re Reynolds number ($= UD/\nu$), dimensionless
- St Strouhal number ($= f_v D/U$), dimensionless
- t time, s
- U free-stream fluid speed, m/s
- $\mathbf{u}$ fluid velocity vector, m/s
- $\mathbf{v}$ cylinder velocity vector, m/s
- x cylinder along-flow displacement, m
- $\mathbf{x}$ cylinder position vector, m
- y cylinder cross-flow displacement, m

Greek Symbols

- μ fluid dynamic viscosity, kg/m s
- ν fluid kinematic viscosity, m^2/s
- Π $= p/\rho + \mathbf{u}\cdot\mathbf{u}/2$, m^2/s^2
- ρ fluid density, kg/m^3
- $\boldsymbol{\omega}$ fluid vorticity vector, m/s m
- ω_n $= 2\pi f_n$, rad/s
- ζ ratio of cylinder damping to critical, dimensionless

Superscripts and Subscripts

- $'$ standard deviation value
- 0 fixed cylinder value

REFERENCES

1. Blackburn, H. M., and Karniadakis, G. E., Two- and Three-Dimensional Simulations of Vortex-Induced Vibration of a Circular Cylinder, 3rd Int. Offshore and Polar Eng. Conf., Singapore, Vol. 3, pp. 715–720, 1993.
2. Ongoren, A., and Rockwell, D., Flow Structures from an Oscillating Cylinder. Part 1. Mechanisms of Phase Shift and Recovery in the Near Wake, *J. Fluid Mech.* **191**, 197–223, 1988.
3. Griffin, O. M., Vortex-Induced Vibrations of Marine Structures in Uniform and Sheared Currents, NSF Workshop on Riser Dynamics, Univ. Michigan, 1992.
4. Orszag, S. A., Israeli, M., and Deville, M. O., Boundary Conditions for Incompressible Flows, *J. Sci. Comput.* **1**(1), 75, 1986.
5. Van Atta, C. W., and Gharib, M., Ordered and Chaotic Vortex Streets Behind Circular Cylinders at Low Reynolds Numbers, *J. Fluid Mech.* **174**, 113–133, 1987.
6. Brika, D., and Laneville, A., Vortex-Induced Vibrations of a Long Flexible Circular Cylinder, *J. Fluid Mech.* **250**, 481–508, 1993.
7. Williamson, C. H. K., and Roshko, A., Vortex Formation in the Wake of an Oscillating Cylinder, *J. Fluids Struct.* **2**, 355–381, 1988.
8. Construction Industry Research and Information Association (CIRIA), Report UR8 (2nd ed.): *Dynamics of Marine Structures*, United Kingdom, 1978.
9. King, R., A Review of Vortex-Shedding Research and Its Application, *Ocean Eng.* **4**, 141–171, 1977.
10. Engineering Sciences Data Unit (ESDU), Item 85038: *Circular-Cylindrical Structures: Dynamic Response to Vortex Shedding*, Part 1, London, 1985.
11. Shariff, K., Pulliam, T. H., and Ottino, J. M., A Dynamical Systems Analysis of Kinematics in the Time-Periodic Wake of a Circular Cylinder, *SIAM Lect. Appl. Math.* **28**, 613–646, 1991.
12. Henderson, R. D., and Karniadakis, G. E., Unstructured Spectral Element Methods for the Incompressible Navier–Stokes Equations, Presented at 8th Int. Conf. Finite Element Methods in Fluids, Barcelona, 1993.

Accepted August 24, 1995